# Innate antimicrobial peptide protects the skin from invasive bacterial infection

**Victor Nizet*, Takaaki Ohtake†‡, Xavier Lauth†‡, Janet Trowbridge†‡, Jennifer Rudisill†‡, Robert A. Dorschner†‡, Vasumati Pestonjamasp†‡, Joseph Piraino§, Kenneth Huttner§ & Richard L. Gallo*†‡**

** Department of Pediatrics; and † Division of Dermatology, University of California, San Diego, California 92161, USA*
*‡ Veterans Affairs San Diego Healthcare System, San Diego, California 92161, USA*
*§ Division of Neonatology, Massachusetts General Hospital, Boston, Massachusetts 02114, USA*

**In mammals, several gene families encode peptides with antibacterial activity, such as the β-defensins and cathelicidins[1–3]. These peptides are expressed on epithelial surfaces and in neutrophils, and have been proposed to provide a first line of defence against infection by acting as 'natural antibiotics'[4,5]. The protective effect of antimicrobial peptides is brought into question by observations that several of these peptides are easily inactivated[6–8] and have diverse cellular effects that are distinct from antimicrobial activity demonstrated *in vitro*[9–13]. To investigate the function of a specific antimicrobial peptide in a mouse model of cutaneous infection, we applied a combined mammalian and bacterial genetic approach to the cathelicidin antimicrobial gene family[14]. The mature human (LL-37)[15] and mouse (CRAMP)[16] peptides are encoded by similar genes (*CAMP* and *Cnlp*, respectively), and have similar α-helical structures, spectra of antimicrobial activity and tissue distribution. Here we show that cathelicidins are an important native component of innate host defence in mice and provide protection against necrotic skin infection caused by Group A *Streptococcus* (GAS).**

To assess directly the function of cathelicidins *in vivo*, we generated mice that are null for *Cnlp* by targeted recombination. A targeting vector was constructed in which exons 3 and 4, encoding the entire mature domain of *CRAMP*, were replaced with PGK-neo flanked 5′ by a genomic Xba/R1 fragment and 3′ by a 5.5-kilobase (kb) R1 fragment of *Cnip* (Fig. 1a). This construct was introduced into 129/SVJ embryonic stem cells by electroporation and subjected to G418 selection. Recombinant clones were screened by polymerase chain reaction (PCR) using a forward primer 5′ to the deletion construct and reverse primer within the neomycin resistance gene. Embryonic stem cell clones were injected into C57BL/6 blastocysts and transferred to foster mothers. Chimaeric offspring were crossed with C57BL/6 females, whose heterozygous progeny were identified by PCR (Fig. 1b), and these were immediately backcrossed into 129/SVJ. Northern blot analysis confirmed the absence of CRAMP in *Cnlp*-null bone marrow (Fig. 1c). *Cnlp*-null mice had normal fetal development, were fertile, survived into adulthood, and demonstrated no obvious phenotype when housed under aseptic barrier-controlled conditions.

The cathelicidins CRAMP and LL-37 (refs 15, 16) are greatly increased in the skin after wounding, owing to their release from neutrophil granules and increased synthesis by keratinocytes[17]. We chose to use GAS for our mouse infection model because the injury accompanying this pathogen leads to a large increase in the local accumulation of CRAMP[17]. Moreover, GAS are highly sensitive to cathelicidin antimicrobial action, even under culture conditions that inactivate peptide killing of other bacteria frequently described as sensitive (for example, *Escherichia coli*)[17]. Subcutaneous injection of GAS in mice induces a necrotic lesion that is histopathologically similar to that seen with invasive human infections. After identical injections of cathelicidin-sensitive GAS in wild-type, heterozygous and homozygous-null mice, CRAMP-deficient mice were observed to develop much larger areas of infection (Fig. 2a, b). Lesion areas increased more rapidly, reached larger maximal size, and persisted longer in CRAMP-deficient mice than in normal littermates while heterozygotes tended to have lesions of intermediate size (Fig. 2c). Cultures of equal amounts of tissue from lesions biopsied at day 7 after injection demonstrated persistent infection with β-haemolytic GAS in CRAMP-deficient mice but not in normal mice (Fig. 2d). No difference in GAS lesion size was seen when wild-type parental strains C57BL/6 and 129/SVJ were compared.

A complementary approach to demonstrating the importance of cathelicidins in host defence is to examine the effects *in vivo* of altering bacterial sensitivity to CRAMP. If the antimicrobial action of cathelicidin is essential to control a GAS skin infection, as suggested by the experiments with *Cnlp*-null mice, then CRAMP-resistant GAS should be more pathogenic than CRAMP-sensitive GAS in normal mice. A transposon mutant library was generated from wild-type GAS strain NZ131 by random integration of Tn*917* into the bacterial chromosome. In contrast to the parent strain, bacterial growth was observed in a pooled library of transposon mutants exposed to increasing concentrations of the cathelicidin antimicrobial peptide. Southern blot analysis of several isolated colonies demonstrated clonality. The sequence flanking the single chromosomal integration of Tn*917* in the cathelicidin-resistant mutant (NZ131-CR)was identified and compared to the recently completed GAS genome database[18]. The Tn*917* insertion mapped to an open reading frame (GenBank AAK34584) encoding a predicted product of relative molecular mass 28,200 ($M_r$ 28.2K) with the signature helix-turn-helix motif of the GntR family of bacterial transcription regulation proteins[19] (Fig. 3a). To demonstrate that Tn*917* disruption at this locus was reproducibly associated with an inducible cathelicidin-resistance phenotype, targeted plasmid integrational mutagenesis of the *gnt*R-related open reading frame was

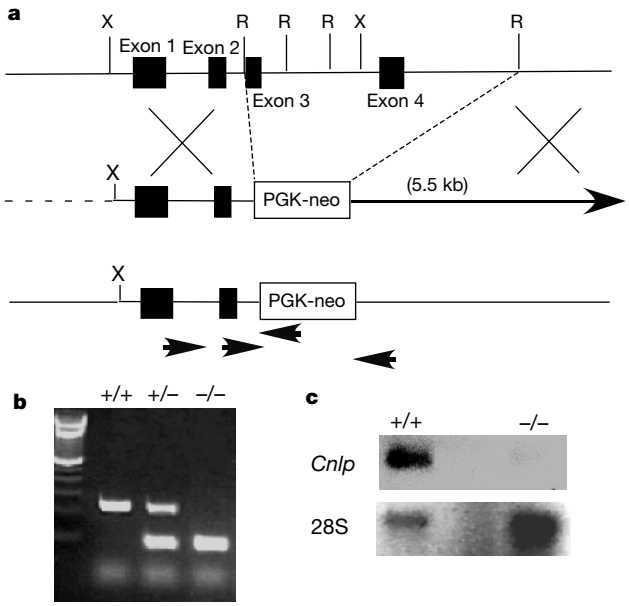


**Figure 1** Disruption of the *Cnlp* gene encoding CRAMP in mice. **a**, Gene targeting strategy: structure and partial restriction map of *Cnlp*. Top line, filled boxes represent exons 1–4. X, *Xho*I; R, *Eco*RI. Second line, Targeting construct replaces exon 3–4 R fragment with PGK-neo and retains 5′ X–R fragment and 5.5-kb 3′ R fragment. Dotted lines, gene fragment replaced by PGK-neo; crosses, flanking regions in construct to target homologous recombination; bottom line, inactivated allele; arrowheads are PCR primers. **b**, PCR genotype results of tail DNA amplified with primers shown in **a**. **c**, Northern blot results of total RNA extracted from bone marrow. *Cnlp* probe is directed to exon 4 alone. 28S RNA is shown as a loading control.

performed in the parent GAS NZ131 (Fig. 3a). The putative cathelicidin-resistance regulatory gene was designated *crg*R (for cathelicidin resistance gene regulator) and the targeted plasmid integrational mutant was designated NZ131:*crg*R.KO. NZ131:*crg*R.KO exhibited inducible CRAMP-resistance to identical minimal inhibitory concentrations (MICs) when compared to the original Tn*917* mutant (Fig. 3b). Comparison of the kinetics of bacterial killing upon exposure to CRAMP further demonstrated that mutant bacteria were resistant to the bactericidal action of the peptide (Fig. 3c). Both the transposon and targeted CRAMP-resistant mutants exhibited slight growth inhibition in enriched culture media compared to the parent GAS strain (data not shown), suggesting a metabolic cost to the bacteria associated with acquired antimicrobial peptide resistance and possible pleiotropic effects of this regulatory gene mutation. We note that mutations in transcriptional regulatory genes of *Salmonella*[20] and *Burkholderia pseudomallei*[21] have also been associated with a change in susceptibility to cationic antimicrobial peptides.

CRAMP-resistant mutants of GAS were compared to wild-type GAS for their ability to produce necrotizing cutaneous infection in a normal mouse model. Mice infected with Tn*917* mutant NZ131-CR or targeted mutant NZ131:*crg*R.KO had lesions of larger size and longer duration than those infected with the parent GAS strain (Fig. 3d–f). Biopsy and quantitative culture of the lesions from mice infected with the CRAMP-resistant mutants showed persistent infection at day 7 in contrast to the microbial clearing observed with the CRAMP-sensitive parent GAS. Thus, cathelicidin-resistant mutants demonstrated increased virulence *in vivo*. In effect, induction of cathelicidin resistance in the bacterial pathogen reproduced the phenotype of the *CRAMP* gene knockout in the mouse infection model.

At day 3, histological examination of GAS-induced skin lesions from CRAMP-deficient mice showed abundant neutrophilic infiltrates comparable to those seen in the wild-type mice (data not shown). No differences were seen in the circulating peripheral leukocyte morphology or count as determined by microscopic examination of blood smears (data not shown) or by fluorescence-activated cell sorting (FACS) analysis (Fig. 4a, b). Furthermore, leukocytes derived from CRAMP-deficient mice were functionally competent and similar to wild-type leukocytes in oxidative burst activity (Fig. 4c). These observations suggest that although CRAMP-deficient mice appear to have normal recruitment of an acute neutrophil inflammatory response, the absence of the antimicrobial peptide in the neutrophil granule and epidermal keratinocyte leads to defects in the control of GAS infection. The importance of CRAMP in phagocytic clearance of GAS was reflected in results of whole-blood killing assays (Fig. 4d). Fresh blood from wild-type mice reduced bacterial counts after incubation for one hour, whereas fresh blood from CRAMP-deficient mice allowed bacterial replication. Bacterial replication was also seen when CRAMP-resistant GAS was incubated in wild-type mouse blood. As expected, the CRAMP-resistant phenotype of GAS did not affect

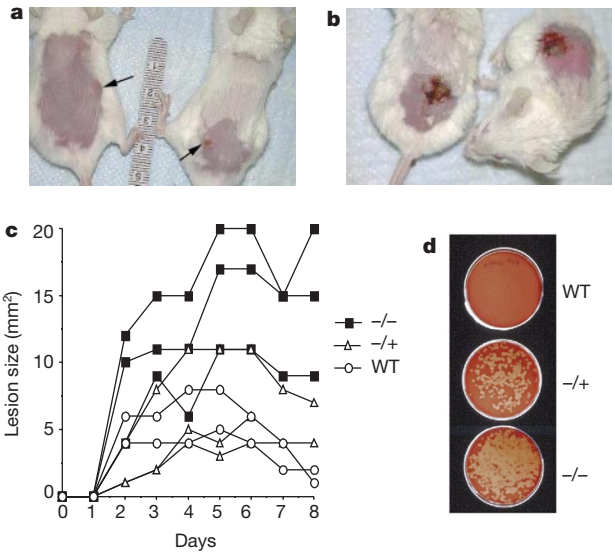


**Figure 2** *Cnlp*-deletion renders mice susceptible to severe GAS infection. **a**, Wild-type (WT) and **b**, *Cnlp*-null mice following subcutaneous inoculation with GAS. Scale bar is in centimetres. **c**, Area of necrotic ulcer in individual WT (circle), CRAMP +/– (triangle), and CRAMP –/– (square) mice shown against days after infection. **d**, GAS bacteria cultured from tissue biopsies of WT, CRAMP –/+ and CRAMP –/– mice. The experiment shown is representative of five studies in which similar differences were observed ($n = 12$, $P < 0.001$).

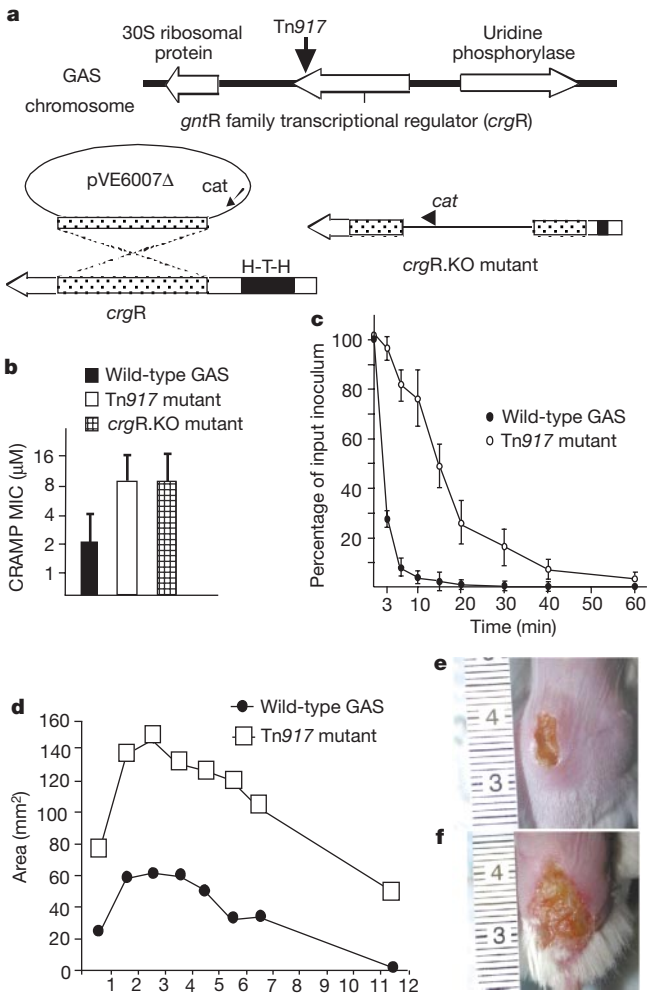


**Figure 3** GAS mutants resistant to CRAMP produce more severe infections in normal mice. **a**, Chromosomal location of the Tn*917* insertion in CRAMP-resistant GAS mutant NZ131:*crg*R.KO. H-T-H, helix-turn-helix; cat, chloramphenicolacetyltransferase. **b**, Minimum inhibitory concentrations of CRAMP against wild-type GAS parent strain NZ131 (black bar), Tn*917* mutant NZ131-CR (white bar), and targeted plasmid integrational mutant NZ131:*crg*R.KO (hatched bar). **c**, Bacterial killing kinetics of 32 μM CRAMP versus wild-type GAS and Tn*917* mutant NZ131-CR. **d**, Area of necrotic ulcer formation in wild-type mice infected with CRAMP-resistant mutant NZ131-CR (square) versus CRAMP-sensitive parent strain NZ131 (circle). Data are means of three mice and similar differences were observed in five experiments with NZ131-CR ($n = 10$, $P < 0.01$) and two experiments with NZ131:*crg*R.KO ($n = 8$, $P < 0.001$). Representative lesions in mice infected with **e**, CRAMP-sensitive parent strain NZ131 versus **f**, CRAMP-resistant mutant NZ131-CR. Scale is shown in centimetres.

the degree of bacterial replication in the blood of CRAMP-deficient mice. Similarly, CRAMP-deficient mice showed no difference in skin lesion size when injected with wild-type or CRAMP-resistant GAS (data not shown).

We have thus demonstrated *in vivo* that endogenous expression of a mammalian antimicrobial peptide provides defence against an invasive bacterial infection. Bacterial resistance to cathelicidins altered disease outcome in a similar fashion to elimination of host cathelicidin production. These paired findings suggest that the specific antimicrobial activity of the cathelicidin is itself necessary for bacterial clearance and innate skin immunity. Some earlier studies[22–25] have also suggested *in vivo* protection by mammalian antimicrobial peptides. For example, inhibition of antimicrobial peptide activation leads to increased wound colonization by *Staphylococcus epidermidis* in pigs[22], natural resistance to antimicrobial peptide action appears to contribute to *Salmonella* virulence in mice[23], downregulation of enteric cathelicidin and β-defensin-1 expression is correlated with *Shigella* infections in humans[24], and improved lung clearance of *Pseudomonas aeruginosa* is associated with overexpression of a human antimicrobial peptide gene in transgenic mice[25]. These observations, combined with our own, suggest that the study of the effects of cathelicidin deficiency at other epithelial surfaces will further define the function of this family of antimicrobial peptides in disease. Other antimicrobial peptides (such as the defensins) that are co-expressed with cathelidicins act synergistically *in vitro*, and may have a similar role *in vivo*. Furthermore, the influence of cathelicidins and defensins on cell-mediated immunity through leukocyte recruitment[26,27] may also contribute to their defense properties. Finally, analysis of the bacterial genetic basis of cathelicidin sensitivity can shed light on the mechanism(s) of action of this class of antimicrobial peptides and the reasons why resistance has not emerged in the evolution of certain pathogenic bacterial species. We believe a combined genetic approach, studying the susceptibility factors of both host and pathogen, to be fruitful in understanding these important components of the innate immune system. □

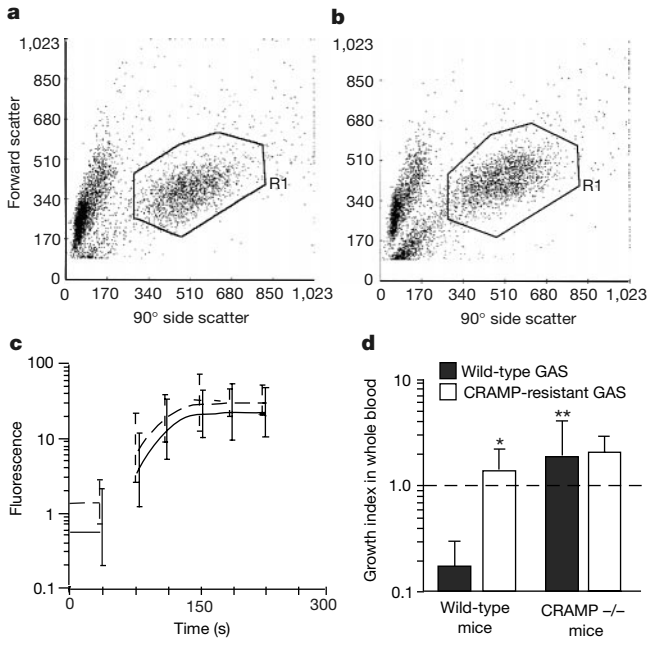


**Figure 4** *Cnlp*-null mouse blood leukocytes are equivalent in relative number and oxidative burst capacity, but deficient in bacterial killing when compared to leukocytes derived from wild-type mice. Flow cytometry of leukocytes derived from **a**, *Cnlp*-null mice and **b**, wild-type mice. Granulocyte population is indicated (R1). Data are representative of the results obtained for seven individuals per genotype. The proportion of leukocytes, monocytes and lymphocytes were not significantly different by analysis with paired *t*-test. **c**, Oxidative burst capacity as measured by fluorescence before (0–40 s) and after (~75–250 s) the addition of a reagent designed to stimulate leukocyte phagocytic and oxidative activity as described in Methods. The mean log fluorescence per time is indicated for wild-type (dashed line) and *Cnlp*-null (solid line) mice with error bars indicating the range of >95% of fluorescent readings collected at each time point. Data are representative of three individual experiments. **d**, GAS killing activity of whole mouse blood. Data are expressed as growth index (c.f.u. bacteria after 1 h incubation in blood versus initial bacterial c.f.u.) and represent the mean of four mice tested in each group. Asterisk, $P < 0.02$; double asterisk, $P < 0.01$ versus normal mouse/wild-type GAS.

## Methods

### Generation of *Cnlp*-deficient mice

*Cnlp*-null mice were generated by targeted disruption of *Cnlp* through homologous recombination. Embryonic stem cell culture and blastocyst injection were performed at Genome Systems (St Louis, Missouri), now Incyte Genomics (Palo Alto, California). Screening for positive recombinant embryonic stem cells was performed by PCR and confirmed by Southern blot. Selected embryonic stem cell clones were karyotyped and two normal clones were used for germline transmission. Male chimaeras were bred with C57BL/6 females and germline mice were identified using PCR analysis with the following *Cnlp* primers: (5′-CCAGGGACTTCCATCCAGTAGAC-3′, 5′-TGTTTTCTCAGATCCTTGGGAGC-3′, 5′-AATTTTCTTGAACCGAAAGGGC-3′) and neo reverse primer (5′-AGACTGCCTTGGGAAAAGCG-3′). Correct insertion was confirmed using a primer 5′ to the Xba site at the start of the targeting construct (5′-GTCAGGTCACATAGG-CAATGGG-3′) and the reverse neo primer. The identity of PCR products was confirmed by direct sequencing. Heterozygote offspring from chimaeric matings were backcrossed into 129/SVJ for two generations.

### Bacterial mutagenesis

GAS strain NZ131 is a well characterized T14/M49 patient isolate that produces the virulence factors streptolysin S and O, and pyrogenic exotoxin (SPE) B[28]. NZ131 was randomly mutated with Tn*917* using the temperature-sensitive delivery vector $pTV_1OK$ (ref. 28). Mutant clone NZ131-CR was identified by Southern analysis following serial passage of the pooled library in increasing concentrations of CRAMP (4–16 μM). Single-primer PCR[29] with a Tn*917*-specific outward primer was used to identify the NZ131-CR mutation site, and a BLAST (http://www.ncbi.nlm.nih.gov/BLAST) homology search against the GAS genome (see http://www.genome.ou.edu/strep.html)[18] revealed identity with the open reading frame we have designated *crg*R. For targeted mutagenesis of *crg*R, an intragenic fragment was amplified by PCR and cloned into the temperature-sensitive vector pVE6007Δ. The resultant 'knockout' plasmid was introduced into NZ131 by electroporation, and chloramphenicol (Cm)-resistant transformants identified at the permissive temperature for plasmid replication (30 °C). Single-crossover Campbell-type chromosomal insertion was selected by shifting to the non-permissive temperature (37 °C) while maintaining Cm selection; fidelity of the site-directed recombination event and disruption of the targeted open reading frame was confirmed by PCR[28].

### Antimicrobial assays

For MIC determination, serial dilutions of the peptide were made in $H_2O$ and 10 μl of each concentration added to replicate wells of a 96-well flat-bottom tissue-culture plate. GAS were grown in Todd Hewitt Broth (THB, Difco) to early log phase (absorbance at 600 nm, $A_{600} = 0.2$). Bacteria were diluted in THB to $A_{600} = 0.001$ (~$2 \times 10^5$ colony-forming units (c.f.u.) $ml^{-1}$). In triplicate, 90 μl of this bacterial suspension was added to each well containing antimicrobial peptide. Growth was monitored at $A_{600}$ through overnight incubation at 37 °C, and MIC was calculated as the lowest peptide concentration yielding no detectable growth. For antimicrobial killing kinetics, ~$2 \times 10^5$ c.f.u. of each strain were exposed to 32 μM CRAMP and incubated at 37 °C. Dilutions were plated at time points from 3 to 60 min for determination of surviving c.f.u.

### Mouse model of GAS infection

Invasiveness of GAS in mouse skin was measured by modification of a previously described GAS infection model[30]. Procedures were approved by the Veterans Affairs (VA) San Diego Healthcare System subcommittee on animal studies. For *Cnlp*-null mice experiments, the backs of sex-matched adult littermates were shaved and hair removed by chemical depilation (Neet) then injected subcutaneously with 50 μl of a mid-logarithmic growth phase ($A_{600} = 0.6$, ~$5 \times 10^7$ c.f.u.) of GAS NZ131 complexed to Cytodex beads as a carrier. For experiments with CRAMP-resistant GAS, 12-week-old Balb/c female mice were similarly prepared and injected with equal numbers of NZ131, NZ131-CR, or NZ131:*crg*R.KO. Lesion sizes were measured daily and statistical significance between groups evaluated by multiple regression analysis on VassarStats (http://faculty.vassar.edu/lowry/VassarStats.html).

### Flow cytometry

Some 200–500 μl of whole blood was collected into 12 ml cold phosphate-buffered saline (PBS) heparin (2 U $ml^{-1}$) (Sigma number H3393). Cells were centrifuged and erythrocytes lysed using Becton Dickinson FACS Lysis Buffer (number 349202). Unlysed cells were washed once with 1 ml DMEM 2% BSA (Sigma number A2153), then resuspended in

200–400 μl 4% paraformaldehyde (PFA) (number S898-07 JT Baker). Approximately $2 \times 10^4$ cells were evaluated for forward and side scatter characteristics by flow cytometry under the direction of J. Nordberg at the VA Core Flow Facility to determine the relative percentage of lymphocytes, monocytes and granulocytes. For oxidative burst assay, blood was collected and lysed as above then resuspended at 4 °C in approximately 200 μl endotoxin and pyrogen-free PBS without $Ca^{2+}$ and $Mg^{2+}$ (number 70013-032, Gibco BRL) containing 5 mM glucose (Sigma number G5146). Before the oxidative burst assay, 200 μl of PBS at 37 °C containing 1.5 mM $Mg^{2+}$ and 1.0 mM $Ca^{2+}$ was added to the cell suspension. The Fc OxyBURST Green Assay Reagent (Molecular probes number F-2902) was used to evaluate cell uptake and oxidative burst activity. Background fluorescence was recorded, then oxidative burst reagent added to a concentration of 30 μg $ml^{-1}$ (5 μl).

### Whole blood killing assay

Fresh mouse blood was collected as above and 35 μl added to 10 μl of THB containing $(1–2) \times 10^2$ c.f.u of freshly diluted log-phase GAS. The mixture was incubated for 1 h at 37 °C with gentle agitation, and dilutions of the mixture plated on agar plates for enumeration of c.f.u. The growth index was calculated as the ratio of bacterial c.f.u. recovered versus the initial bacterial inoculum. Student's *t*-test analysis was performed using the Microsoft Excel statistical package.

Received 28 June; accepted 1 October 2001.


1. Scott, M. G. & Hancock, R. E. Cationic antimicrobial peptides and their multifunctional role in the immune system. *Crit. Rev. Immunol.* **20,** 407–431 (2000).
2. Boman, H. G. Innate immunity and the normal microflora. *Immunol. Rev.* **173,** 5–16 (2000).
3. Ganz, T. & Lehrer, R. Antibiotic peptides from higher eukaryotes: biology and applications. *Mol. Med. Today* **5,** 292–297 (1999).
4. Ganz, T. *et al.* Defensins: natural peptide antibiotics of human neutrophils. *J. Clin. Invest.* **76,** 1427–1435 (1985).
5. Zasloff, M. Magainins, a class of antimicrobial peptides from *Xenopus* skin: Isolation, characterization of two active forms, and partial cDNA sequence of a precursor. *Proc. Natl Acad. Sci. USA* **84,** 5449–5453 (1987).
6. Goldman, M. J. *et al.* Human β-defensin-1 is a salt-sensitive antibiotic in lung that is inactivated in cystic fibrosis. *Cell* **88,** 553–560 (1997).
7. Wang, Y., Agerberth, B., Lothgren, A., Almstedt, A. & Johansson, J. Apolipoprotein A-I binds and inhibits the human antibacterial/cytotoxic peptide LL-37. *J. Biol. Chem.* **273,** 33115–33118 (1998).
8. Travis, S. M. *et al.* Bactericidal activity of mammalian cathelicidin-derived peptides. *Infect. Immun.* **68,** 2748–2755 (2000).
9. Gallo, R. L. *et al.* Syndecans, cell surface heparan sulfate proteoglycans, are induced by a proline-rich antimicrobial peptide from wounds. *Proc. Natl Acad. Sci. USA* **91,** 11035–11039 (1994).
10. Shi, J., Ross, C., Leto, T. & Blecha, F. PR-39, a proline-rich antibacterial peptide that inhibits phagocyte NADPH oxidase activity by binding to Src homology 3 domains of $p47^{phox}$. *Proc. Natl Acad. Sci. USA* **93,** 6014–6018 (1996).
11. Lencer, W. *et al.* Induction of epithelial chloride secretion by channel-forming cryptdins 2 and 3. *Proc. Natl Acad. Sci. USA* **94,** 8585–8589 (1997).
12. Risso, A., Zanetti, M. & Gennaro, R. Cytotoxicity and apoptosis mediated by two peptides of innate immunity. *Cell. Immunol.* **189,** 107–115 (1998).
13. Chertov, O. *et al.* Identification of defensin-1, defensin-2, and CAP37/azurocidin as T-cell chemoattractant proteins released from interleukin-8-stimulated neutrophils. *J. Biol. Chem.* **271,** 2935–2940 (1996).
14. Zanetti, M., Gennaro, R., Scocchi, M. & Skerlavaj, B. Structure and biology of cathelicidins. *Adv. Exp. Med. Biol.* **479,** 203–218 (2000).
15. Gudmundsson, G. H. *et al.* The human gene *Fall39* and processing of the cathelin precursor to the antibacterial peptide LL-37 in granulocytes. *Eur. J. Biochem.* **238,** 325–332 (1996).
16. Gallo, R. L. *et al.* Identification of CRAMP, a cathelin-related antimicrobial peptide expressed in the embryonic and adult mouse. *J. Biol. Chem.* **272,** 13088–13093 (1997).
17. Dorschner, R. A. *et al.* Cutaneous injury induces the release of cathelicidin antimicrobial peptides active against group A *Streptococcus*. *J. Invest. Dermatol.* **117,** 91–97 (2001).
18. Ferretti, J. J. *et al.* Complete genome sequence of an M1 strain of *Streptococcus pyogenes*. *Proc. Natl Acad. Sci. USA* **98,** 4658–4663 (2001).
19. Peekhaus, N. & Conway, T. Positive and negative transcriptional regulation of the *Escherichia coli* gluconate regulon gene *gntT* by GntR and the cyclic AMP (cAMP)–cAMP receptor protein complex. *J. Bacteriol.* **180,** 1777–1785 (1998).
20. Miller, S. I., Pulkkinen, W. S., Selsted, M. M. & Mekalanos, J. J. Characterization of defensin resistance phenotypes associated with mutations in the phoP virulence regulon of *Salmonella typhimurium*. *Infect. Immun.* **58,** 3706–3710 (1990).
21. Burtnick, M. N. & Woods, D. E. Isolation of polymyxin B-susceptible mutants of *Burkholderia pseudomallei* and molecular characterization of genetic loci involved in polymyxin B resistance. *Antimicrob. Agents Chemother.* **43,** 2648–2656 (1999).
22. Cole, A. M. *et al.* Inhibition of neutrophil elastase prevents cathelicidin activation and impairs clearance of bacteria from wounds. *Blood* **97,** 297–304 (2001).
23. Groisman, E. A., Parra-Lopez, C., Salcedo, M., Lipps, C. J. & Heffron, F. Resistance to host antimicrobial peptides is necessary for *Salmonella* virulence. *Proc. Natl Acad. Sci. USA* **89,** 11939–11943 (1992).
24. Islam, D. *et al.* Downregulation of bactericidal peptides in enteric infections: A novel immune escape mechanism with bacterial DNA as a potential regulator. *Nature Med.* **7,** 180–185 (2001).
25. Bals, R., Weiner, D., Meegalla, R. & Wilson, J. Transfer of a cathelicidin peptide antibiotic gene restores bacterial killing in a cystic fibrosis xenograft model. *J. Clin. Invest.* **103,** 1113–1117 (1999).
26. De, Y. *et al.* LL-37, the neutrophil granule- and epithelial cell-derived cathelicidin, utilizes formyl peptide receptor-like 1 (FPRL1) as a receptor to chemoattract human peripheral blood neutrophils, monocytes, and T cells. *J. Exp. Med.* **192,** 1069–1074 (2000).
27. Yang, D. *et al.* β-defensins: linking innate and adaptive immunity through dendritic and T cell CCR6. *Science* **286,** 525–528 (1999).
28. Nizet, V. *et al.* Genetic locus for streptolysin S production by group A streptococcus. *Infect. Immun.* **68,** 4245–4254 (2000).
29. Karlyshev, A. V., Pallen, M. J. & Wren, B. W. Single-primer PCR procedure for rapid identification of transposon insertion sites. *Biotechniques* **28,** 1078–1082 (2000).
30. Betschel, S., Borgia, S., Barg, N., Low, D. & De Azavedo, J. Reduced virulence of group A streptococcal Tn916 mutants that do not produce streptolysin S. *Infect. Immun.* **66,** 1671–1679 (1998).



### Acknowledgements

This work was supported by grants from the NIH (R.L. G. and V. N.), a VA merit award (R.L.G.), and grants from the American Skin Association (R.L.G.) and the Rockefeller Brothers Foundation (V.N.).


Correspondence and requests for materials should be addressed to R.L.G. (e-mail: rgallo@vapop.ucsd.edu).

# The E2F1–3 transcription factors are essential for cellular proliferation

**Lizhao Wu*, Cynthia Timmers*, Baidehi Maiti*, Harold I. Saavedra*, Ling Sang*, Gabriel T. Chong*, Faison Nuckolls†, Paloma Giangrande†, Fred A. Wright*, Seth J. Field‡, Michael E. Greenberg‡, Stuart Orkin§, Joseph R. Nevins†, Michael L. Robinson‖ & Gustavo Leone***

** Division of Human Cancer Genetics, Department of Molecular Virology, Immunology and Medical Genetics, and Department of Molecular Genetics; and ‖ Division of Molecular and Human Genetics, Children's Research Institute, The Ohio State University, Columbus, Ohio 43210, USA*
*† Department of Genetics, Howard Hughes Medical Institute, Duke University Medical Center, Durham, North Carolina 27710, USA*
*‡ Department of Neuroscience, § Howard Hughes Medical Institute, Children's Hospital, Harvard Medical School, Boston, Massachusetts 02115, USA*

**The retinoblastoma tumour suppressor (Rb) pathway is believed to have a critical role in the control of cellular proliferation by regulating E2F activities[1,2]. E2F1, E2F2 and E2F3 belong to a subclass of E2F factors thought to act as transcriptional activators important for progression through the G1/S transition[3]. Here we show, by taking a conditional gene targeting approach, that the combined loss of these three E2F factors severely affects E2F target expression and completely abolishes the ability of mouse embryonic fibroblasts to enter S phase, progress through mitosis and proliferate. Loss of E2F function results in an elevation of $p21^{Cip1}$ protein, leading to a decrease in cyclin-dependent kinase activity and Rb phosphorylation. These findings suggest a function for this subclass of E2F transcriptional activators in a positive feedback loop, through down-modulation of $p21^{Cip1}$, that leads to the inactivation of Rb-dependent repression and S phase entry. By targeting the entire subclass of E2F transcriptional activators we provide direct genetic evidence for their essential role in cell cycle progression, proliferation and development.**

The delineation of a pathway controlling the progression of cells out of quiescence, through G1 and into S phase, has been established[1,2]. Principal events in this pathway include the activation of cyclin-dependent kinases (CDKs), the coordinated phosphorylation of Rb and p130 by cyclin–CDK complexes, and the subsequent release and accumulation of E2F activities[1,2]. Although E2F has an essential role in control of cell growth during *Drosophila* development[4,5], current knockout mouse models have failed to demonstrate a similar requirement for any E2F family member in mammals[6–12]. One interpretation of these observations is that under normal circumstances, loss of a single E2F member can be functionally compensated by other related E2F activities.

Of the six known E2F family members, E2F1, E2F2 and E2F3 can specifically interact with Rb, and their expression is cell-cycle regulated[13,14]. To test for functional redundancy among this subclass